International Research Journal on Advanced Engineering and Management
https://goldncloudpublications.com
https://doi.org/10.47392/IRJAEM.2026.0221
e ISSN: 2584-2854
Volume: 04 Issue: 05
May 2026
Page No: 1473 - 1477

Structural and Optical Study of Tb3+ Substituted in Cobalt Ferrite Nanoparticles by The Sol-Gel Auto-Combustion Method

Kranti Prakashrao Hasnalkar[1], Arati Chandragupta Mehere[2], Sanchita Vishwas Chavan[3], Bhise Ramesh Baburao[4], Sopan Mansing Rathod[5]
[1]Department of Physics, PDEA's Annasaheb Magar Mahavidyalaya, Hadapsar, Pune, Maharashtra, India.
[2,5]Advanced Materials and Nanotechnology Research Laboratory, Department of Physics, MES Abasaheb Garware College, Pune, Maharashtra, India.
[3,4]DGM's, hon. Balasaheb Jadhav Arts, Commerce and Science College, Ale, Junnar, Pune-412411, Maharashtra, India.
Email id: *krantiphasnalkar@gmail.com[1]*

Abstract
Structural and optical properties of Tb3+ doped TbxCoFe2-xO4 (where X= 0.025, 0.075, 0.1) spinel ferrites were successfully synthesized by the sol-gel auto combustion method and sintered at 400 ℃ for 4 hours in an air atmosphere. The X-ray diffraction pattern confirms the formation of a cubic spinel phase structure. The average crystalline size was determined to be between to nm and both the lattice parameters and crystalline size decreased as the Tb3+ concentration increased. The intense 330 peaks show the single-phase formation of the ferrite sample. Morphological analysis through Scanning Electron Microscopy (SEM) shows spherical structure.
Keywords: *Ferrites, Spinel, Cobalt.*

1. Introduction
A broad family of oxides known as ferrites has exceptional structural and magnetic characteristics [1]. Both practically and fundamentally, ferrites are important and fascinating materials [2]. Due to their unique chemical, optical, magnetic, electrical, and dielectric properties as well as their structural and thermal stability, nanosized CoFe2O4, MnFe2O4, ZnFe2O4, NiFe2O4 and CuFe2O4 have drawn a lot of attention among other ferrites. These properties also have a wide range of potential technological applications, including photoluminescence, photocatalysis, humidity sensors, biosensors, pigment, corrosion protection, antimicrobial agents and biomedicine [3-8]. Cobalt ferrite bulk material's microstructure is significantly impacted by rare earth elements such as La, Sm, Gd, Dy, Er and Yb. Cobalt is a significant and adaptable element with a wide range of uses in several industries. Cobalt-based catalysts are vital for a number of chemical processes, such as the creation of hydrogen, organic synthesis, and petroleum refining [9,10].Various morphologies, such as nanoparticles, hollow mesoporous nanospheres, nanorods, and three-dimensional organised microporous structures, have been investigated in the production of CoFe2O4 [9–11]. Terbium is a useful rare earth element with a wide range of uses in sectors including electronics, lighting, and energy. It has unique magnetic and optical characteristics. Because of its unique properties, terbium is a vital component in sophisticated technologies and is still being researched for potential advances [12]. The typical formula for nickel ferrite (NiFe2O4), along with a spinel structure is AB2O4 [13], where all of the Ni ions are found as the B (octahedral) site and the iron ions are found respectively at the A (tetrahedral) site along with B sites [14]. Due to its great mechanical hardness, huge permeability at high frequencies, low cost, chemical stability, and increased electric resistivity, nickel ferrite is widely employed in electronic devices [15]. NiFe2O4's magnetic and dielectric characteristics are heavily influenced by its

International Research Journal on Advanced Engineering and Management
https://goldncloudpublications.com
https://doi.org/10.47392/IRJAEM.2026.0221
e ISSN: 2584-2854
Volume: 04 Issue: 05
May 2026
Page No: 1473 - 1477

cation distribution and manufacturing process [16-19]. It has been investigated how to alter ferrites at the atomic level using several kinds of nonmagnetic [20-24] and magnetic [25] atoms for cations. Ferrite's crystal structure is altered by this selection, which also has an impact on the Fe3+–O2−–Fe3+ interaction.

2. Synthesis Method

TbxCoFe2-xO4 (where X=0.025, 0.075, 0.1) nano ferrite was prepared by the sol-gel auto-combustion method. The AR grade ferric nitrate ((Fe(NO3)2.9H2O), cobalt nitrate, terbium nitrate ((Tb(NO3)2.5H2O and ammonium hydroxide solution were used. The citric acid C6H8O7.H2O was used as fuel. The nitrates and citric acid in a stoichiometric proportion are dissolved in 100 ml distilled water, which is stirred till a homogeneous solution is obtained. The ammonium hydroxide solution is added drop by drop till Ph is equal to 7 is obtained. Then the mixed solution was kept on a hot plate at 100◦C for 1-2 hours to obtain the sol of it. after half an hour, this sol becomes a viscous gel. The gel then burns automatically to get the ash of ferrite nanoparticles. The ash was grinded in an agate mortar to get fine powder. Later, the powder was sintered at 400 ◦C for 4 hours in the muffle furnace in an air atmosphere.

3. Results and Discussion

3.1.X-Ray Diffraction (XRD)

The X-ray diffraction (XRD) pattern of the Tb3+doped Co spinel ferrite nanoparticles with TbCoxFe2O4, where x = 0.025, 0.075 and 0.1 was synthesized by the sol-gel auto-combustion method. The XRD analysis is used to reveal the formation of crystalline phase structure and lattice constants. In the XRD pattern, the broad peaks indicate the fine nature of the particles. The average crystalline size was determined between to nm. And both the crystalline phase and lattice parameter decrease as the Tb3+ concentration increases. The observed peaks (222), (400), (332), (532), (631), and (642) confirm the cubic spinel structure of the samples. The XRD data was used to calculate lattice parameter (a), crystal size (D), lattice strain (), x-ray density of the most intense XRD pattern (400) of ferrite samples by using equations (1) to ().

$$a = d$$

where d is the interplanar distance and h, k, l are the Miller indices. The crystalline size was calculated using the Debye–Scherrer formula,

$$D = \frac{k\lambda}{\beta\cos\theta} \qquad (1)$$

The average crystalline size (D) and lattice strain () were also calculated using the Williamson–Hall (W-H) equation, which is given as,

$$\beta = \frac{K\lambda}{D\sin\theta} + 4\varepsilon\tan\theta \qquad (2)$$

$$D = \frac{K\lambda}{(\text{Intercept})} \qquad (3)$$

$$\varepsilon = \text{Slope} \qquad (4)$$

Where e is lattice strain, D is crystalline size, λ is the wavelength of the X-ray used, β is the full width at half maximum and θ is the Bragg's angle. As Shown in Figure 1.

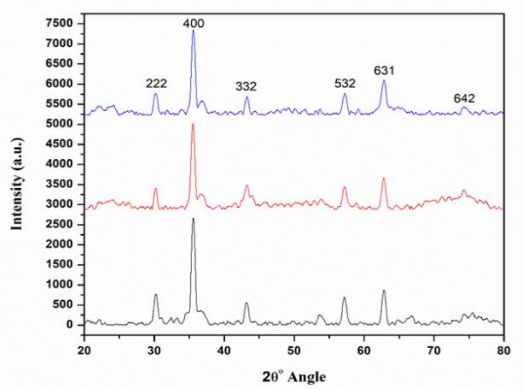

Figure 1 X-ray diffraction (XRD) patterns of TbxCoFe2-xO4 at (x= 0.025, 0.075, 0.1)

3.2.UV- Visible Spectroscopy

The absorbance spectra show a clear dependence on

International Research Journal on Advanced Engineering and Management
https://goldncloudpublications.com
https://doi.org/10.47392/IRJAEM.2026.0221
e ISSN: 2584-2854
Volume: 04 Issue: 05
May 2026
Page No: 1473 - 1477

composition (x) across the wavelength range of 200–800 nm. All samples exhibit strong absorption in the UV region, followed by a broad absorption band extending into the visible region, and a gradual decrease toward the near-infrared region. As Shown in Table 1.

Table 4 EDX of $Tb_xCoFe_{2-x}O_4$ at (x= 0.00)

Element	Line	Mass %	Atom%
Fe	k	64.01±3.12	65.24±3.18
Co	k	35.99±2.64	34.76±2.55
Tb	Line	nd	nd
Total		100	100
Spc_001			Fitting ratio 0.4966

The sample with x = 0.025 displays the highest absorbance throughout the spectrum, with a prominent peak around 320–350 nm, indicating stronger electronic transitions. As the composition increases to x = 0.075 and x = 0.1, the overall absorbance decreases, and the spectra become comparatively flatter, suggesting a reduction in the number of absorbing species or changes in the electronic structure. As Shown in Figure 2.

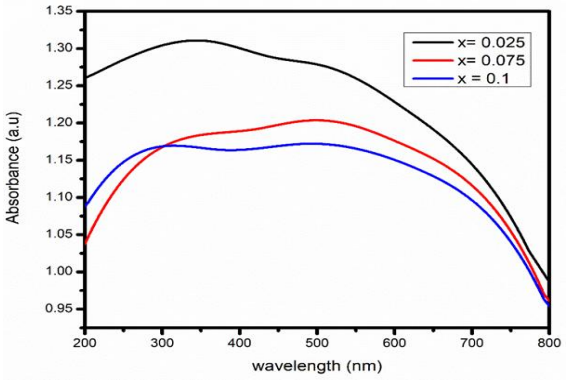

Figure 2 UV–Vis DRS of TbxCoFe2-xO4 at (x= 0.025, 0.075, 0.1)

A slight shift of the absorption feature toward longer wavelengths is also observed with increasing x, which may indicate band gap narrowing or modification in energy levels. In the higher wavelength region (700–800 nm), all samples show a sharp decline and tend to converge, indicating minimal absorption and increased transparency. Overall, the results suggest that increasing x significantly influences the optical properties of the material by reducing absorbance and slightly altering the absorption edge.

3.3.SEM analysis

The SEM micrographs of TbxCoFe2-xO4 at (x= 0.00) presented in Fig.3, effectively illustrate the synthesis's outcomes. The images reveal a modest degree of agglomeration, characterized by a spherical morphology that contributes to a spherical structure. This non-uniform distribution can be attributed to various factors, including reaction time and sintering temperature. Interestingly, the observed agglomeration of nanoparticles likely results from their magnetic behaviour and the relatively weak surface interactions among primary particles, which are primarily held together by Van der Waals forces. As Shown in Figure 3 & 4.

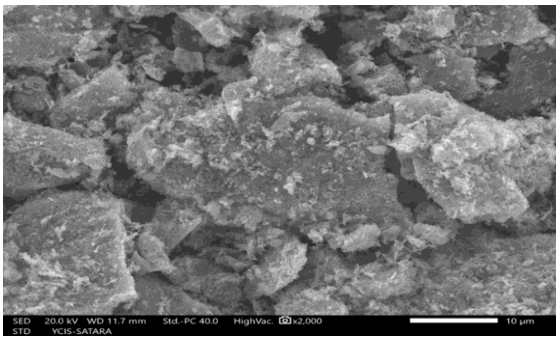

Figure 3 SEM of TbxCoFe2-xO4 at (a) x=0.00

International Research Journal on Advanced Engineering and Management
https://goldncloudpublications.com
https://doi.org/10.47392/IRJAEM.2026.0221
e ISSN: 2584-2854
Volume: 04 Issue: 05
May 2026
Page No: 1473 - 1477

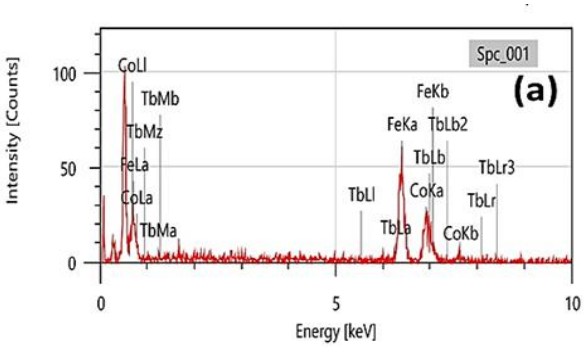

Figure 4 EDX of TbxCoFe2-xO4 at x=0.00

Conclusion

In this present work, the Nanocrystalline TbxCoFe2O4 (where x = 025, 0.075, 0.1) powder was successfully synthesized by sol gel auto combustion method. The XRD pattern confirms the formation of a cubical spinel phase structure. The average grain size was determined to be between to nm. And both the lattice parameters and crystalline size decrease as the Tb3+ concentration increases. The intense 330 peaks show the single-phase formation of the ferrite sample. , the results suggest that increasing x significantly influences the optical properties of the material by reducing absorbance and slightly altering the absorption edge. . The images reveal a modest degree of agglomeration, characterized by a spherical morphology that contributes to a spherical structure.

References

[1]. R. Valenzuela, Magnetic Ceramics, Cambridge University Press, 2005
[2]. Chand P., Vaish S., Kumar P. Structural, optical and dielectric properties of transition metal (MFe2O4; M = Co, Ni and Zn) nanoferrites. Phys. B Condens Matter. 2017;524:53–63.
[3]. Asghar K., Qasim M., Das D. Preparation and characterization of mesoporous magnetic MnFe2O4@mSiO2 nanocomposite for drug delivery application. Mater. Today Proc. 2020;26:87–93
[4]. Sivakumar P., Ramesh R., Ramanand A., Ponnusamy S., Muthamizhchelvan C. Synthesis and characterization of NiFe2O4 nanoparticles and nanorods. J. Alloy Comp. 2013;563:6–11.
[5]. Ozçelik B., Ozçelik S., Amaveda H., Santos H., Borrell C.J., Saez-Puche R., de la Fuente G.F., Angurel L.A. High speed processing of NiFe2O4 spinel using laser furnance. J. Materiomics. 2020;6:661–670.
[6]. Džunuzović A.S., Ilić N.I., Vijatović Petrović M.M.V., Bobić J.D., Stojadinović B., Dohčević-Mitrović Z., Stojanović B.D. Structure and properties of Ni–Zn ferrite obtained by auto-combustion method. J. Magn. Magn. Mater. 2018;374:245–251.
[7]. Kaur H., Singh A., Kumar A., Ahlawat D.S. Structural, thermal and magnetic investigations of cobalt ferrite doped with Zn2+ and Cd2+ synthesized by auto combustion method. J. Magn. Magn. Mater. 2019;474:505–511.
[8]. Naik A.B., Naik P.P., Hasolkar S.S., Naik D. Structural, magnetic and electrical properties along with antifungal activity & adsorption ability of cobalt doped manganese ferrite nanoparticles synthesized using combustion route. Ceram. Int. 2020;46:21046–21055.
[9]. Xiong, Q.Q.; Tu, J.P.; Shi, S.J.; Liu, X.Y.; Wang, X.L.; Gu, C.D. Ascorbic acid-assisted synthesis of cobalt ferrite (CoFe2O4) hierarchical flower-like microspheres with enhanced lithium storage properties. J. Power Sources 2014, 256, 153–159.
[10]. Li, X.; Sun, Y.; Zong, Y.; Wei, Y.; Liu, X.; Li, X.; Peng, Y.; Zheng, X. Size-effect induced cation redistribution on the magnetic properties of well-dispersed CoFe2O4 nanocrystals. J. Alloy Comp. 2020, 841, 155710.
[11]. Manikandan, A.; Sridhar, R.; Arul, S.A.; Ramakrishna, S. A simple aloe vera plant-extracted microwave and conventional combustion synthesis: Morphological, optical, magnetic and catalytic properties of CoFe2O4 nanostructures. J. Molec. Struct. 2014, 1076, 188–200.
[12]. Deepa Guragain , Binod Kumar Rai ,

International Research Journal on Advanced Engineering and Management
https://goldncloudpublications.com
https://doi.org/10.47392/IRJAEM.2026.0221
e ISSN: 2584-2854
Volume: 04 Issue: 05
May 2026
Page No: 1473 - 1477

Sunghyun Yoon , Tej Prasad Poudel , Subash Chandra Bhandari and Sanjay R Mishra
[13]. 1. Pérez, E.; Marquez, G.; Sagredo, V. Effect of calcination on characteristics of nickel ferrite nanoparticles synthesized by sol-gel method. Iraqi J. Appl. Phys. 2019, 15, 13–17.
[14]. Dixit, G.; Negi, P.; Singh, J.P.; Srivastava, R.C.; Agrawal, H.M. Effect of Ce Doping on the Magnetic Properties of NiFe2O4 Nanoparticles. J. Supercond. Nov. Magn. 2013, 26, 1015–1019. [CrossRef]
[15]. Singhal, S.; Chandra, K. Cation distribution and magnetic properties in chromium-substituted nickel ferrites prepared using aerosol route. J. Sol. State Chem. 2007, 180, 296–300. [CrossRef]
[16]. Krishna, K.R.; Ravinder, D.; Kumar, K.V.; Lincon, C.A. Synthesis, XRD & SEM studies of zinc substitution in nickel ferrites by citrate gel technique. World J. Cond. Matt. Phys. 2012, 2, 153.
[17]. Dormann, J.L.; Nogues, M. Magnetic structures in substituted ferrites. J. Phys. Cond. Matt. 1990, 2, 1223. [CrossRef]
[18]. Rezlescu, N.; Rezlescu, E.; Pasnicu, C.; Craus, M.L. Effects of the rare-earth ions on some properties of a nickel-zinc ferrite. J. Phys. Cond. Matt. 1994, 6, 5707.
[19]. Virden, A.E.; O'Grady, K. Structure and magnetic properties of NiZn ferrite nanoparticles. J. Magn. Magn. Mater. 2005, 290, 868–870. [CrossRef]
[20]. Batoo, K.M. Microstructural and Mössbauer properties of low temperature synthesized Ni-Cd-Al ferrite nanoparticles. Nanoscale Res. Let. 2011, 6, 499. [CrossRef]
[21]. Sharma, R.K.; Suwalka, O.P.; Lakshmi, N.; Venugopalan, K. Hyperfine fields in nano particles of Cr0.25Co0.25Zn0.5Fe2O4 . Indian J. Pure Appl. Phys. 2007, 45, 830–833.
[22]. Wang, L.; Rai, B.K.; Mishra, S.R. Structural and magnetic study of Al3+ doped Ni0.75Zn0.25Fe2−xAlxO4 nanoferrites. Mater. Res. Bull. 2015, 65, 183–194. [CrossRef]
[23]. Borhan, A.I.; Iordan, A.R.; Palamaru, M.N. Correlation between structural, magnetic and electrical properties of nanocrystalline Al3+ substituted zinc ferrite. Mater. Res. Bull. 2013, 48, 2549–2556. [CrossRef]
[24]. Hashim, M.; Kumar, S.; Ali, S.; Koo, B.H.; Chung, H.; Kumar, R. Structural, magnetic and electrical properties of Al3+ substituted Ni–Zn ferrite nanoparticles. J. Alloy. Compd. 2012, 511, 107–114. [CrossRef]
[25]. Lakhani, V.K.; Zhao, B.; Wang, L.; Trivedi, U.N.; Modi, K.B. Negative magnetization, magnetic anisotropy and magnetic ordering studies on Al3+-substituted copper ferrite. J. Alloy. Compd. 2011, 509, 4861–4867. [CrossRef]
[26]. Lakhani, V.K.; Pathak, T.K.; Vasoya, N.H.; Modi, K.B. Structural parameters and X-ray Debye temperature determination study on copper-ferrite-aluminates. Solid State Sci. 2011, 13, 539–547. [CrossRef]
[27]. Sharifi, I.; Shokrollahi, H. Structural, magnetic and Mössbauer evaluation of Mn substituted Co–Zn ferrite nanoparticles synthesized by co-precipitation. J. Magn. Magn. Mater. 2013, 334, 36–40. [CrossRef]